Pressure Side Tip Platform Extensions for Tip Leakage Control in Axial Turbines

Cengiz Camci*
Turbomachinery Aero-Heat Transfer Laboratory,
Department of Aerospace Engineering,
Pennsylvania State University, PA16802, USA
E-mail: cxc11@psu.edu
*Corresponding author

Akamol Shavalikul
Turbomachinery Aero-Heat Transfer Laboratory,
Department of Aerospace Engineering,
Pennsylvania State University, PA16802, USA
E-mail: azs180@psu.edu

Abstract: Pressure side extensions are effective tip leakage control devices in axial flow turbines. RANS based viscous flow simulations are used to compare a number of potential aerodynamic de-sensitization devices for blade tips. The present study is a continuation of the past aerodynamic experiments performed in the rotating turbine rig at the Pennsylvania State University by Dey and Camci (2004). After a brief discussion of the computational details, a grid independency study is presented. The current study shows that a significant tip leakage mass flow rate and aerodynamic loss reduction is possible by using proper tip platform extensions located near the pressure side corner of the blade tip. A set of computations with realistic turbine rotor inlet flow conditions are performed in a linear cascade arrangement in the relative frame of reference. The boundary conditions for the computations are obtained from inlet flow measurements performed in Penn State Axial Flow Turbine Research Facility AFTRF.

Keywords: tip leakage flow, turbine, CFD, pressure side tip extension

Biographical notes:

C. Camci is currently a Professor of Aerospace Engineering at the Pennsylvania State University. He obtained his doctoral degree from the von Karman Institute for Fluid Dynamics in Belgium in 1985. He directed research in the Turbomachinery Aero-heat Transfer Laboratory at Penn State since 1986. He teaches theory of turbomachinery, fluid dynamics, turbulent flow, aerospace propulsion, propulsion systems for un-inhabited air vehicles and finite element methods in fluid dynamics and heat transfer. C.Camci is a Fellow of the ASME, American Society of Mechanical Engineers.

S. Akamol is a graduate research assistant at the Turbomachinery Aero-heat transfer Laboratory at Pennsylvania State University. He received his MSc. in thermal power from Cranfield University, UK in 2001. He is pursuing PhD. in Aerospace engineering at the Pennsylvania State University.

1 INTRODUCTION

Over tip leakage flow is responsible from a significant amount of aerodynamic loss in a turbine stage. Most shroud less turbine rotor designs require a gap between blade tip and casing. A comprehensive summary of the over tip leakage aerodynamics is provided by Denton (1993). The pressure difference between the pressure side and the suction side induces the leakage flow across the tip. The over tip gap flow mixes with the mainstream passage flow. The interaction of this flow results in the generation of a secondary leakage vortex near the blade suction side corner that contains a significant loss core. Denton and Cumpsty (1987) describes the effects of tip leakage flow. The leakage

flow passes over the blade tip essentially without being turned. Consequently, the blade force and the work done are reduced. Tip leakage flow does not go through the usual expansion process occurring at mid-span region of the turbine passage. The leakage fluid mixing with the core flow is relatively hotter than the core fluid because of this inherent "*lack of work extraction*" in the tip clearance region. Bindon (1988) explains how this mixing generates the aerodynamic loss. The mixing loss is typically intense within the last 40% chord length region where the fluid does not have sufficient momentum to compensate the diffusion. The flow starts to separate from the suction side corner and form a large vortical structure. The leakage flow that has the significant vortical content interacts and mixes with near casing flow, passage vortex and the blade wake flow. A tip loss model developed by Denton (1993) is given in Equation 1. There are several possible means of reducing the over tip leakage flow related loss ζ, at a given relative tip clearance level t/*h*.

$$\zeta = \frac{2C_d}{\cos\beta_2}\left(\frac{t}{h}\right)\left(\frac{c}{s}\right)\int_0^1 \left(\frac{V_s}{V_2}\right)^3\left(1-\frac{V_p}{V_s}\right)\left[1-\left(\frac{V_p}{V_s}\right)\right]^{1/2}\frac{dz}{c} \qquad (1)$$

1. Reducing the discharge coefficient Cd
2. Modifying the rotor exit conditions
3. Changing the aerodynamic characteristics of the blade tip for raising the pressure side velocity Vp or reducing the suction side velocity Vs
4. Increasing the pitch-chord ratio s/c

1.1 Reducing the discharge coefficient C_d:

A number of studies have explored this option. Booth (1985) conducted an experiment by using a water flow discharge rig to study the effects of tip geometry on the discharge coefficient C_d. According to this experiment, the knife edge geometry had the lowest C_d of 28% that was below the flat tip value. Bindon et al. (1988) presented experimental results that were obtained in a linear cascade facility at a fixed relative gap height. When the blade tip corner radius was increased a C_d value that was 12 % higher than the blade with a plain tip was obtained. This contoured tip can reduce the flow contraction at the blade tip and the mixing loss near the suction surface. The methods, which concentrate only on reducing C_d, may not be appropriate for lower over tip leakage loss. Heyes et al. (1991) studied the over tip leakage flow in two linear cascade arrangements. The effects of using plain tip, suction side squealer and pressure side squealer were investigated. They found that the suction side squealer gave the best reduction in C_d. The use of squealer tips for reducing tip leakage mass flow rate and loss have been reported by a number of researchers in various aspects. Camci et al. (2005) showed the experimental investigation of aerodynamic characteristics of full and partial squealer rims using the Axial Flow Turbine Research Facility AFTRF at Pennsylvania State University. Various lengths of a few squealer rims along the chordwise direction were investigated to reach the minimum of the aerodynamic loss. Their experimental observations from the rotating turbine rig AFTRF indicated that implementation of partial squealer rims positively affected the local aerodynamic performance by weakening the tip vortex. The term "weakening the tip vortex" was equivalent to a reduction in the momentum deficit contained in the tip vortex area. Prakash et al. (2006) provided a numerical investigation of a conventional squealer tip with a straight shelf and inclined shelf near the pressure side in an effort to control the leakage flow. The computations showed that the specific shelf designs applied to the pressure side of the tip region were highly effective in weakening the tip vortex. More recent experiments performed in the rotating rig AFTRF also confirmed the beneficial influence of similar inclined shelf designs.

1.2 Modifying the rotor exit conditions:

The aerodynamic characteristics of turbine blades are modified either increasing the relative exit velocity V_2 or reducing the relative angle β_2. Yamamoto et al. (1994) and Dececco et al. (1995) reported that the off-loading the tip, which can change the rotor exit conditions, is able to reduce the over tip leakage flow.

1.3 Changing the aerodynamic characteristics of the blade tip:

This approach is based on raising the pressure side velocity V_p or reducing the suction side velocity V_s. Partial shroud (winglet) geometry has the potential for increasing the pressure side velocity V_p. Patel (1998) performed an experimental investigation of partial shroud tips and showed that the partial shroud tip can improve the stage efficiency by 1.2%. Booth et al. (1985) studied several partial shroud geometries in a water cascade rig. The double winglet design was the most proficient design which can improve the stage efficiency by +0.6 %. Yaras and Sjolander (1991) investigated three different winglet geometries, pressure side winglet, suction side winglet and the double-sided winglet. The specific winglet geometries reduced the over tip leakage loss by 10%. Harvey and Ramsden (2000) presented a novel design of partial shroud geometry derived from a review of past research. The winglet was predicted to significantly improve the turbine stage efficiency, by 1.2 to 1.8% at 2% relative gap height t/h. Dey and Camci (2004) performed an experiment for investigating the effects of the winglet geometries upon the over tip leakage flow structure. The experimental results from the rotating rig AFTRF showed that the pressure side extension (bump) geometry was highly effective to obtain effective over tip leakage control.

1.4 Increasing the pitch-chord ratio s/c:

Denton (1993) investigated the effect of changing the pitch-chord ratio, from *s/c* of 0.9 to 0.45, on the over tip leakage loss. For a given exit angle $\beta_2 \geq 60^\circ$ and inlet angle $\beta_1 \leq 0^\circ$, the over tip leakage decreased by 50%. Harvey and

Ramsden (2000) compared the over tip loss at s/*c* values of 1.14 and 0.57. For exit angle $\beta_2 \geq 60^\circ$ and inlet angle of 0 degree and less, the over tip leakage loss was significantly reduced by more than 44%. However, it is not practical to achieve lower tip leakage loss by increasing the number of rotor blades. Other sources of loss increase as well as the cost, weight and complexity of the cooling system.

The current study deals with the concept of controlling the tip leakage by using pressure side tip extension geometries. This concept was introduced by Camci et al. (2005) in an experimental investigation focusing on the pressure and suction side tip platform extensions in a rotating turbine rig. It was found that properly designed pressure side extensions can reduce the over tip leakage flow mass flow rate and associated loss. Since the tested suction side tip platform extensions were not effective in reducing the tip leakage mass flow rate, the current computational effort focused on pressure side tip platform extensions. The numerical simulations of the flow for a linear cascade arrangement are performed to obtain the general characteristics of specific tip leakage flow patterns. The flow field details in the tip gap area are currently difficult to resolve by means of conventional aerodynamic experimental tools. Computational simulations of tip gap flow could be beneficial in understanding leakage flow physics although the absolute accuracy of current computations may not be as good as conventional aerodynamic measurement systems. The set of computational simulations for the geometries defined in Figure 1 are as follows:

1. Baseline geometry, flat tip with out pressure side extension.
2. Bump tip, which is the same as Camci and Dey's (2005) pressure side tip extension geometry.
3. Parallel pressure side extension tip; the width of the extension along the periphery is kept constant.
4. The modified-bump No.1; this geometry is obtained by shifting the tip extension of the bump tip to 50% axial chord length.
5. The modified-bump No.2; this geometry is obtained by expanding the tip extension of the bump tip from 40% to 60% axial chord length.

2 NUMERICAL ANALYSIS

2.1 Governing equations:

The three dimensional, steady, turbulent form of the Reynolds-averaged Navier-Stokes equations are solved by a finite volume formulation using a general purpose viscous flow solver. The rotor isothermal viscous flow calculations are performed in the relative frame of reference using measured rotor inlet conditions in the turbine rig AFTRF. The goal of the simulations is to assess the relative total pressure change as a measure of the aerodynamic performance of the rotor. The continuity equation and momentum equations are shown in Equations 2 and 3, respectively.

$$\frac{\partial U_i}{\partial x_i} = 0 \qquad (2)$$

$$\rho U_j \frac{\partial U_i}{\partial x_j} = -\frac{\partial p}{\partial x_i} + \mu \frac{\partial^2 U_i}{\partial x_j \partial x_j} + \frac{\partial(-\rho \overline{u_i u_j})}{\partial x_j} \qquad (3)$$

2.2 Turbulence model:

From Equation 3, the Reynolds stress tensor $-\rho\overline{u_i u_j}$ components are modeled by using the Boussinesq hypothesis.

$$-\rho\overline{u_i u_j} = -\rho \frac{2}{3} k \delta_{ij} + \mu_t \left(\frac{\partial U_i}{\partial x_j} + \frac{\partial U_j}{\partial x_j}\right) \qquad (4)$$

The standard k-ε model, proposed by Launder and Spalding, is employed to model the turbulence. The Reynolds stress is modeled in terms of two turbulence parameters, the turbulent kinetic energy k and the turbulent energy dissipation rate ε. The turbulent kinetic energy equation is shown in Equation 5.

$$\rho U_i \frac{\partial k}{\partial x_i} = \mu_t \left(\frac{\partial U_j}{\partial x_i} + \frac{\partial U_i}{\partial x_j}\right) \frac{\partial U_j}{\partial x_i} + \frac{\partial}{\partial x_i}\left\{\left(\mu + \frac{\mu_t}{\sigma_k}\right)\frac{\partial k}{\partial x_i}\right\} - \rho\varepsilon \qquad (5)$$

The standard smooth-wall functions, proposed by Launder and Spalding, are used to represent the near wall flow characteristics. The law-of-the-wall for mean velocity yields as the following equation.

$$\frac{U_p C_\mu^{1/4} k_p^{1/2}}{\tau_w / \rho} = \frac{1}{K} \ln(E y^*) \qquad \text{where} \qquad y^* = \frac{\rho C_\mu^{1/4} k_p^{1/2} y_p}{\mu} \qquad (6)$$

2.3 Discretization and grid system:

The governing equations are solved by using a finite volume technique with a second-order upwind discretization scheme. All simulations in this study are performed by using the commercially available general purpose flow solver Fluent 6.3.

Figure 3 represents the grid system, which is equivalent to the linear cascade version of a turbine passage in AFTRF. The pitch-chord ratio of the cascade is s/c=0.833. The non-dimensional tip gap is t/h =2% where blade height h = 123 mm. The pitch to chord ratio of the linear cascade is s/c=0.99. The passage flow details of this cold flow turbine are presented in Lakshminarayana, Camci, Halliwell and Zaccaria (1992). These unstructured grids as shown in Figure 3 with grid-clustering in the near wall and tip gap region are generated by using the general purpose grid generator software Gambit. The simulations performed in this study correspond to a Reynolds number of 291,000 based on axial chord length at the tip diameter and mass averaged inlet velocity. The turbine outer casing in this linear cascade computation is defined as a moving wall to simulate the blade rotation. The imposed relative velocity of the casing is computed from the AFTRF rotational speed of N=1320 rpm with respect to the blade.

2.4 Boundary conditions:

Four types of boundary conditions are implemented around the computational region.

Inlet: The measured inlet mean velocity and turbulence profiles, obtained from past AFTRF experiments are used as inlet boundary conditions in this computational study. A sub-miniature five-hole probe having an overall maximum diameter of 1.3 mm is used in the measurements of all three mean velocity components. The measured tangential, axial, and radial components of velocity profile are presented in Figure 2. The total and tangential velocity plots show a decrease in velocity near H = 0.1 and 0.8, due to the hub and tip wall secondary flows. Because of the existence of an endwall boundary layer, the axial velocity profile shows a decrease near the endwalls. The value of inlet k and ε

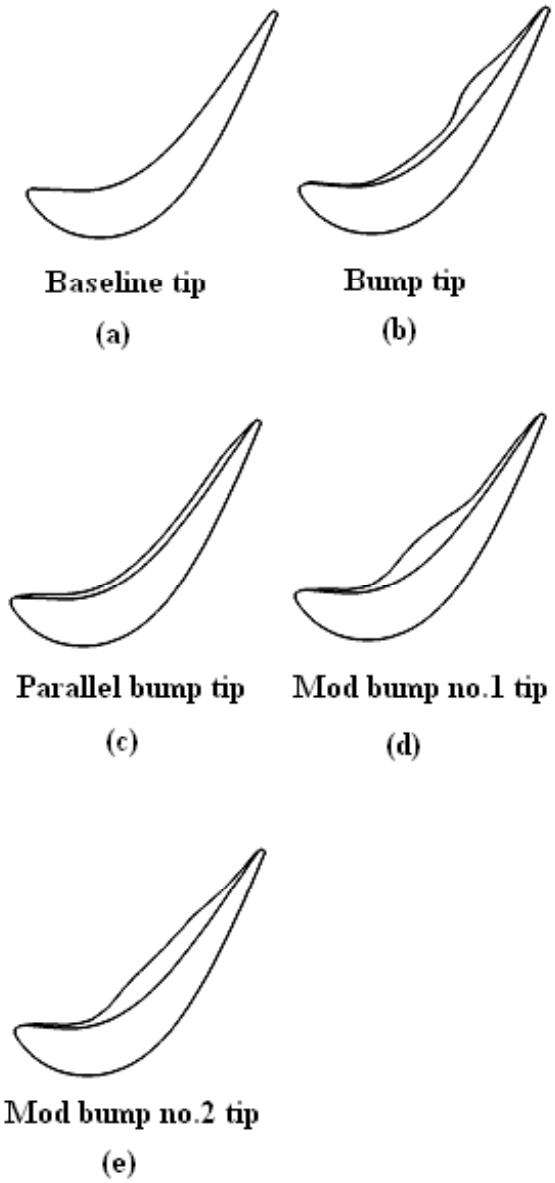

Figure 1 *Schematic of the tip geometries*

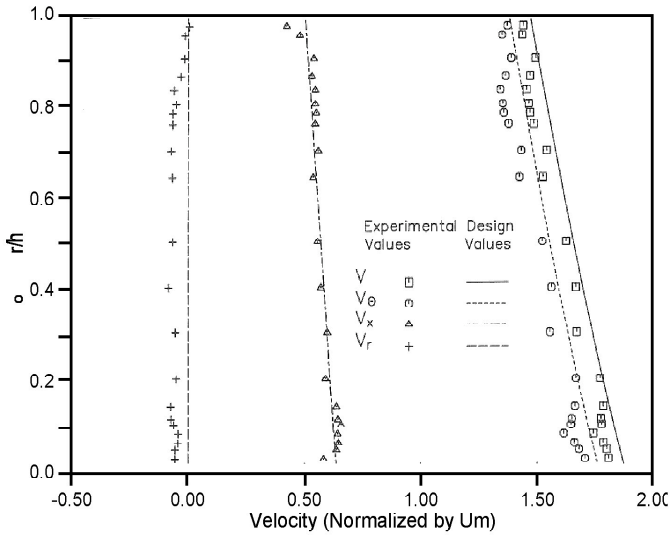

Figure 2 *Measured and design values of axial, tangential and radial velocity components at AFTRF rotor inlet plane*

profiles imposed in this study are based on turbulent intensity and turbulent length scale measurements obtained from the AFTRF by Lakshminarayana, Camci, Halliwell, and Zaccaria, (1992) .

Exit: An outflow boundary condition is used at the exit where all streamwise gradients of computed quantities are imposed as negligible. All of velocity and turbulent quantities are calculated at the exit plane directly. There are no direct enforcements of exit boundary conditions. To satisfy this type of boundary condition, the exit plane should be located far downstream of the rotor trailing edge. In this study, the exit plane is located approximately two chord length downstream of the blade trailing edge.

Solid surface: All of solid surfaces have a no-slip boundary condition and zero turbulent kinetic energy except the outer casing surface facing the rotor tip. The velocity in the tangential direction is set to a constant to simulate endwall relative motion in the planar geometry.

Periodic boundaries: The rotor blade passage flow is periodic. This property considerably simplifies the flow computations. The flow only needs to be resolved in one blade passage having periodic boundaries in circumferential direction. The flow at the periodic boundary as through the opposing periodic plane is a direct neighbor to the cells adjacent to the first periodic boundary.

2.5 Convergency and grid independency:

The acceptable convergence of all cases is achieved when all parameters residual levels are lower than the order of 10^{-5}. The converged simulations needed approximately 1,000 iterations. To find the appropriate grid density, a grid independency study is performed. The grid independency is checked by comparing all solutions of the baseline tip from 3 different grid densities which are 720,000, 1,000,000

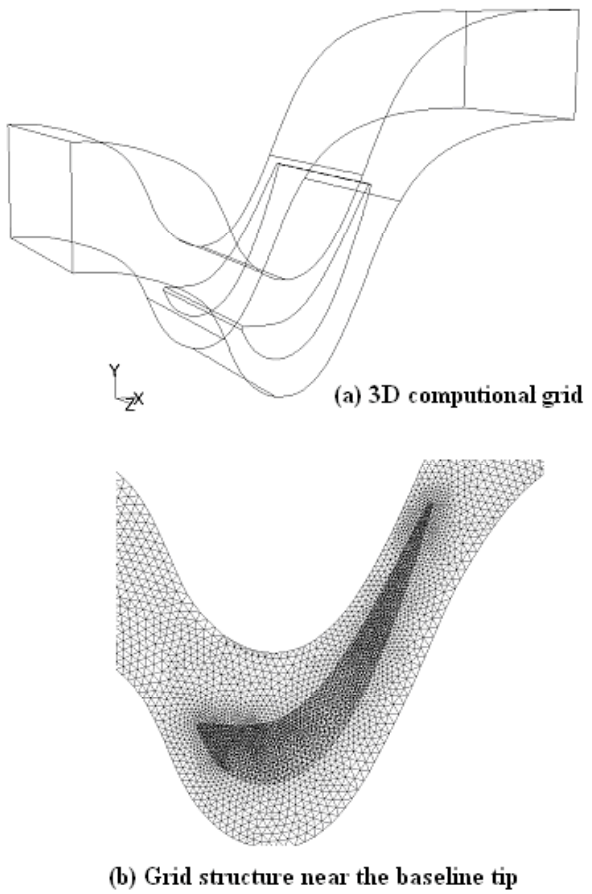

Figure 3 *Schematic of the grid for the flow simulation*

and 1,200,000 grid nodes. The static pressure coefficient at 50% blade height of all different grid densities are plotted in Figure 4. It can be seen that the suction side static pressure at 720,000 grid nodes case has a grid dependent solution. When the grid density is increased to 1,000,000 a significant change in the pressure distribution is observed. Once 1,000,000 grid node number is exceeded, the solution becomes grid independent. To achieve a good level of grid independency, all simulations in this study are thus undertaken by using 1,000,000 grid nodes.

3 RESULTS AND DISCUSSSION

3.1 Static pressure distribution on the tip surface: Referring to many over tip leakage investigations, the pressure difference of the suction side and the pressure side can drive the flow through the tip gap. Thus, the static pressure distributions on the tip platform are of prime importance. In this section, the effects of the different tip geometry on the pressure distribution are examined. The pressure distribution is quantified by using the static pressure coefficient C_p, as defined in Equation 7. The C_p distributions on blade tip platform clearly show the extent of the pressure driven flow, the separation zone near the pressure side corner and trailing edge region where pressure on both pressure side and suction side are very close to each other.

$$C_p = \frac{P - P_{inlet}}{0.5 \times \rho \times V_{inlet}^2} \qquad (7)$$

A large and negative value of the pressure coefficient C_p corresponds to a low pressure difference and vice versa. Thus, the area which has the lower value of C_p would have more potential for the tip leakage drive (green and blue zones).

Figure 5 depicts the static pressure coefficient contours on the blade tip for the baseline and other "pressure side extension" designs. It shows that the first 20% axial chord length from the leading edge region has almost uniform C_p values meaning that the amount of over tip leakage flow in this area is relatively low. The red-orange zone near the leading edge does not have strong pressure gradients to result in significant tip leakage. The high level of over tip leakage flow, which is represented in regions with blue-green color, occurs in between 20% and 70% of axial chord length region. The last 20% axial chord length region near the trailing edge experiences a relatively low tip leakage flow. The C_p distribution on the blade tip especially near the pressure side corner is visibly modified by the pressure side extension tip designs. Dark blue zones at the leakage flow entrance areas near the pressure side corner are almost eliminated in modified bump designs as shown in Figure 5 (d) and (e).

The pressure side extensions generate relatively higher static pressure in the pressure side corner region. The dark blue color apparent in the dominant leakage region of the baseline tip, changes to the light blue color (even green) for all pressure side extensions. The dark blue zone near the pressure side corner is an indication of relatively high

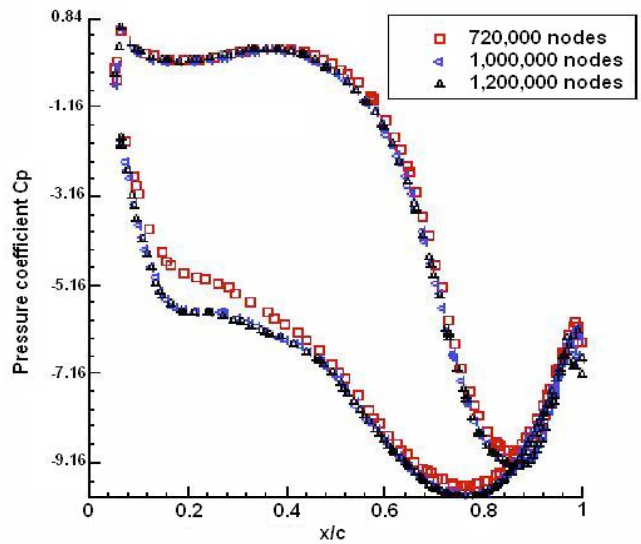

Figure 4 *Grid independency study, the static pressure at 50% blade height*

leakage mass flow rate. The elimination of this dark blue color is an indication of better tip leakage control.

3.1.1 Bump tip:

A comparison of the baseline tip and the bump tip shown in Figure 5a and 5b indicates that the dominant tip leakage region (dark blue) of the bump tip is smaller than that of the baseline tip. As a result of the smaller tip leakage dominant area, the mass flow rate of over tip leakage decreases. However, the pressure distributions from the baseline tip and bump tip shown in Figure 5 suggested that further improvements to limit the leakage mass flow rate are still possible. Other pressure side extension geometries are designed to minimize the leakage mass flow rate in the tip gap area.

3.1.2 Parallel extension tip:

Figure 1 and 5c show the parallel extension tip where the pressure side extension has almost constant width from the leading edge to trailing edge region. This design was generated with the expectation that bump tip's leakage control features could be repeated in other chordwise positions of the tip profile. Parallel extension tip results in a visible improvement in leakage control when compared to bump tip and baseline tip, as observed from Figure 5.

3.1.3 Modified bump No.1 tip:

Moving the pressure side extension of the bump tip to the lowest *Cp* location of the baseline tip can also be a possible option to reduce the tip leakage flow characteristic as seen in modified bump No. 1 tip as shown in Figure 5.d. According to Figure 5.c, the parallel extension tip can eliminate the narrow dark blue zone observed near the pressure side corner in Figure 5.b. The leakage region still covers a wide area. However, Figure 5.c indicates a weakened leakage flow zone in the gap area. The very low static pressure zone (dark blue) apparent near the pressure side corner in general is a measure of the mass flow rate of the leakage flow entering into the tip gap region. When the leakage flow turns around the pressure side corner, it is known that there is a narrow flow separation zone and possible attachment near the pressure side corner. Modified bump No.1 tip design effectively eliminates very low static pressures resulting from significant leakage mass flow rate.

3.1.4 Modified bump No.2 tip:

This design idea is based on the fact that the individual leakage control features of the "*bump tip*" and "*modified bump No.1 tip*" could be effectively combined into one tip extension design. A much wider tip platform extension with a wider chordwise coverage as shown in Figure 5.e is incorporated from *x/c=0.2* to *x/c=0.8*. There is no dark blue color contained in the C_p contour map of the "*modified bump No.2 tip*" indicating that the excessive leakage or high flow acceleration around the pressure side corner is under control. The extent of the dark blue areas near the pressure side corner is an indication of the strength of the leakage flow passing from the tip gap region.

3.2 Mass flow rate across the tip gap:

As a quantitative evaluation, the local over tip leakage mass flow rate across the tip platform camberline is plotted in function of axial chord length ratio in Figure 6. The evaluation is performed over equally formed rectangular areas aligned with the camberline of the tip profile. The computed leakage velocity vectors are integrated over individual rectangular areas to determine the local leakage mass flow rate passing from the tip gap region over the camberline. The leakage mass flow rate continually increases from the leading edge to a maximum value around *x/c=0.65* for the baseline tip. The peak leakage location and the amount of the maximum leakage mass flow rate are different for the *"bump tip"* and "*parallel extension tip*". The mass flow rate at the trailing edge region falls rapidly after *x/c=0.85*. The specific design of the tip platform extension does not influence the local leakage mass flow rate after *x/c=0.85*. The "*bump tip*" and "*parallel extension*

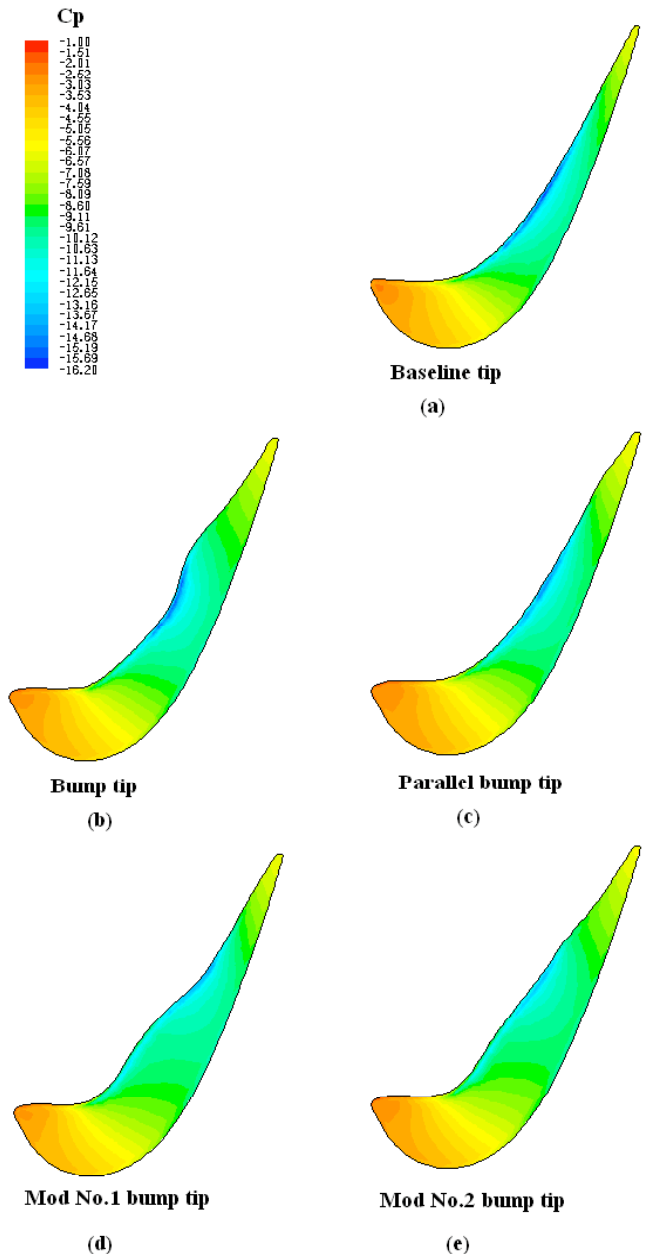

Figure 5 *Contours of static pressure coefficient on the blade tip surface*

tip" local leakage character is the same before *x/c=0.70*. Both treatments provide a considerable gain in reducing tip leakage mass flow rate. The "*bump tip*" alone is an effective treatment only between *x/c=0.70* and 0.*85*. When the location of the extension is moved towards the leading edge, the "*modified bump No.1 tip*", a highly effective leakage reduction is obtained for the mid chord area between *x/c=0.40* and *0.70*. The most effective leakage reduction is obtained in a much wider area using the "*bump tip*" and "*modified bump No.1 tip*". This new design is named "*modified bump No.2 tip*" and it provides effective leakage reduction between *x/c=0.35* and *0.85*.

When the computed local mass flow rates shown in Figure 6 are integrated over the tip gap boundary defined along the blade tip camberline as shown in Table 1, the baseline tip case has the maximum leakage mass flow rate. Reduced leakage mass flow rates can be obtained from all of the

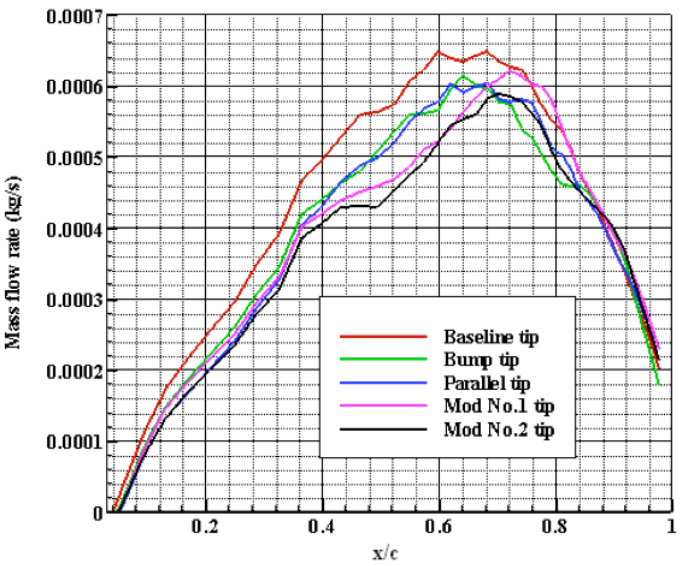

(a)

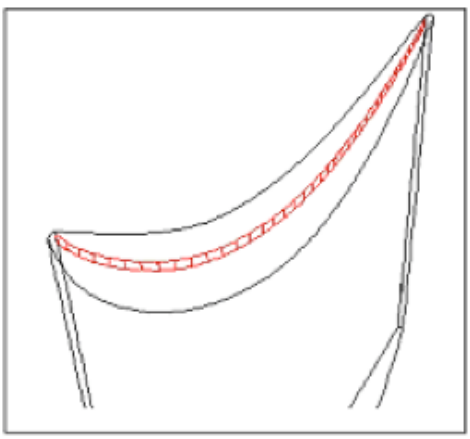

Tip leakage mass flow rate calculation planes

(b)

Figure 6 *The mass flow rate across the tip gap*

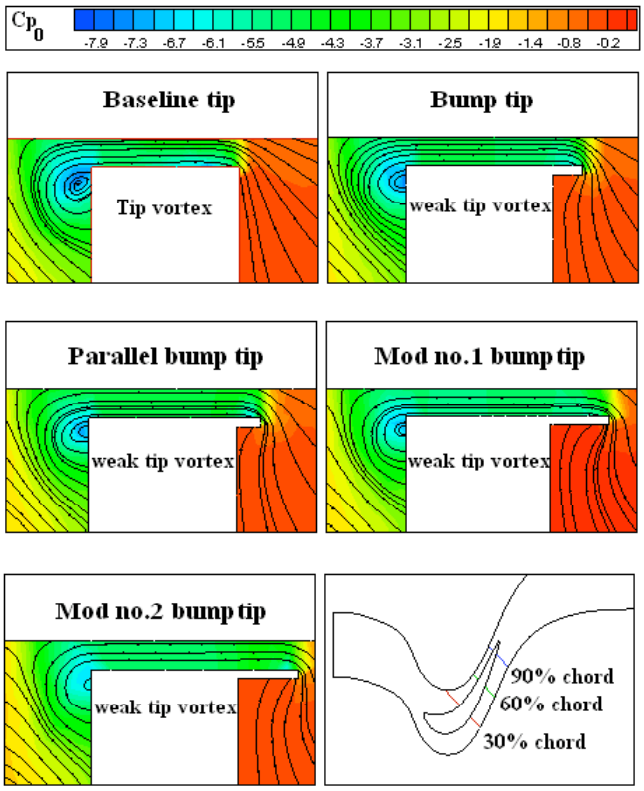

Figure 7 *Leakage flow patterns in the visualization plane at x/c=0.30*

pressure side extension tip geometries presented in Figure 1. Figure 6 shows that, the maximum tip leakage flow region of the "*baseline tip*", the "*bump tip*" and the "*parallel extension tip*" are almost at the same location at about *x/c=0.60*. The high tip leakage region of the "*modified bump No.1 tip*" and "*modified bump No.2 tip*" are shifted to 70 % chord length.

	Mass flow rate (kg/sec)
Baseline tip	0.01757
Bump tip	0.01606
Parallel bump tip	0.01613
Mod. No.1 bump tip	0.01626
Mod. No.2 bump tip	0.01552

Table 1 *Mass flow rate over the blade tip camberline planes*

3.3 Re-circulatory tip flow patterns in cross-stream planes :

Figures 7, 8 and 9 depict computationally generated flow visualization patterns inside three selected planes located at *x/c=0.30, 0.60* and *0.90* respectively. Figure 7 shows the exact alignment of the three visualization planes. The visualization planes are defined as planes that are approximately normal to the passage flow direction. The visualization planes are aligned such that they

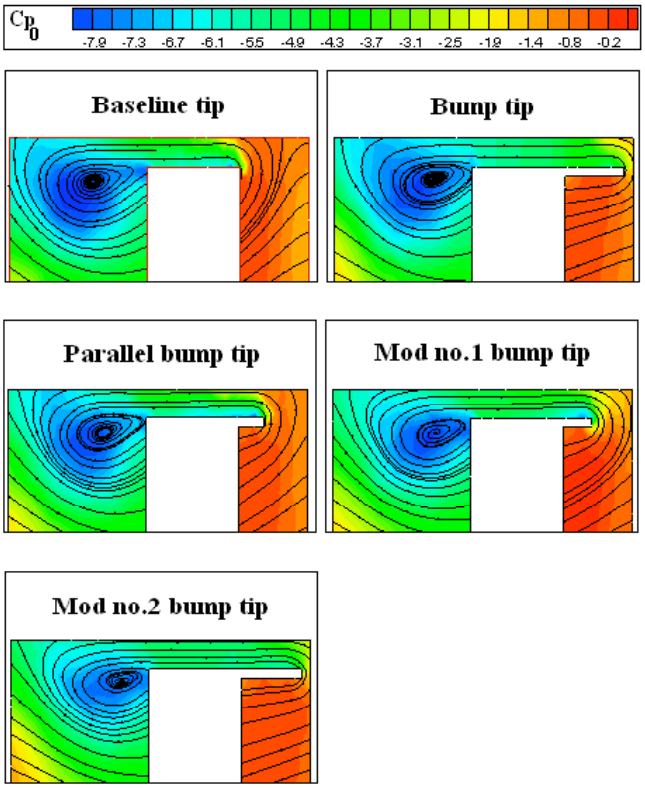

Figure 8 *Leakage flow patterns in the visualization plane at x/c=0.60*

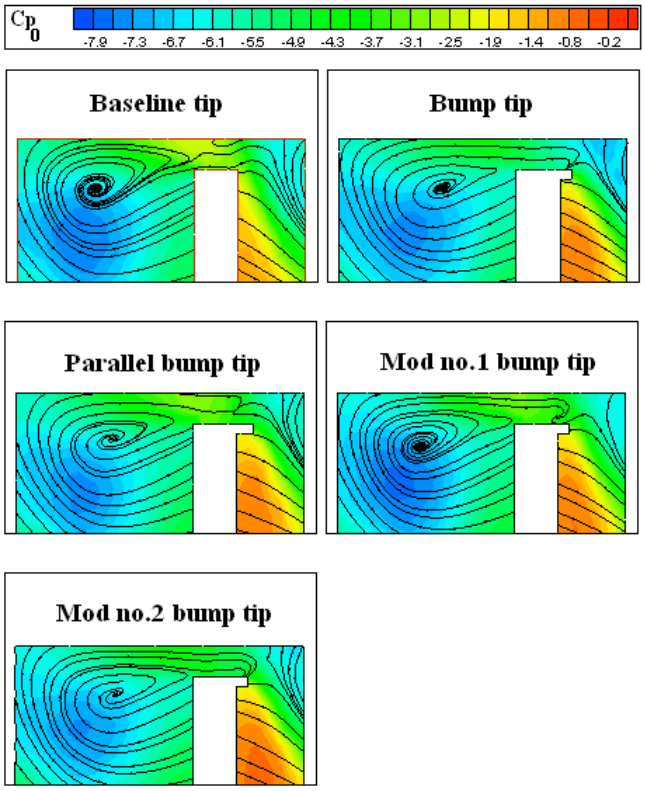

Figure 9 *Leakage flow patterns in the visualization plane at x/c=0.90*

contain most of the tip leakage flow patterns originating from the pressure side corner. The leakage flow is from the right hand side (PS) of each figure to left hand side (SS) corner. The leakage flow entrance area near the pressure side corner of the tip and the interaction of the leakage jet emanating from the tip gap area, its interaction with the passage vortex and the casing wall are contained in selected planes. The visualizations are generated by using the pathlines that are computed based on the velocity components in the visualization plane. The solid colors are for the total pressure coefficient C_{p0}. The numerically generated pathlines based flow visualizations are conceptually equivalent to "smoke flow visualizations" obtained on extremely thin laser sheets that are normal to the blade tip platform. The total pressure coefficient is described as follows:

$$C_{p0} = \frac{P_{total} - P_{total,inlet}}{0.5 \times \rho \times V_{inlet}^2} \qquad (8)$$

3.3.1 Modified tip vortex structure at *x/c=0.30*:

The leakage flow patterns of all tip extension geometries obtained at *x/c=0.30* are similar to the baseline tip results except the gap entrance region. The specific tip platform extension geometry near the pressure side corner determines the shape of entrance area pathlines. The tip leakage flows from the pressure side to suction side of the blade and then mixes with the main passage flow generating a tip vortex. The four specific treatments displayed in Figure 7 all show a slight reduction on the strength of the tip vortex because of the tip platform extensions. The dark blue zone in the core of the resulting tip vortex becomes a light blue region indicating that the total pressure deficit in the core of the baseline tip is slightly reduced in all four treatments.

3.3.2 Modified tip vortex structure at *x/c=0.60*:

A significant amount of tip leakage flow normally mixes with the main passage flow and generates a strong tip vortex for the baseline tip as shown in Figure 8. The tip vortex dominated area at *x/c=0.60* contains higher momentum deficit and energy loss over a larger area when compared to *x/c=0.30*. The bump tip geometry and the parallel extension tip geometry provide a visible reduction in the area coverage of the tip vortex in comparison the baseline tip. The momentum deficit (dark blue zone) in the core of the tip vortex is also visibly recovered. Thus, these suggested blade tip geometries are able to reduce the overall leakage mass flow rate and the aerodynamic losses associated with the tip vortex residing near the suction side corner of the blade. Furthermore, the modified No.1 and modified No.2 bump tips produce the smallest size of the tip vortices and their cores move toward the suction side surface.

3.3.3 Modified tip vortex structure at *x/c=0.90* :

Figure 9 presents the leakage flow patterns inside the visualization plane at *x/c=0.90*. Even though the over tip leakage flow mass flow rate in the trailing edge region is relatively small, the level of loss is extremely high. Figure 9 shows the large vortex and the high negative total pressure coefficient cover almost the whole cross section plane. The

tip vortices for all geometries are now located further away from the blade tip. At *x/c=0.90,* the leakage mass flow rate from the pressure side to suction side corner is much smaller compared to planes located at *x/c= 0.60* and *0.30*. The tip vortex core is large at this station mainly because of the previous leakage mass flow contributions that already formed a distinct tip vortex structure well before *x/c=0.90* location. Comparisons of the results from the five tip platform designs indicate that the lowest level of total pressure loss occurs when modified bump No.2 tip geometry is used. The total pressure contours and the computed pathlines do not coincide at this location. Because of the significant reduction of the leakage mass flow rate in the trailing edge zone, the local leakage mass flow rate is not significant. The local cross stream velocities in the trailing edge area are minimal. However, the tip vortex structure already defined at earlier stations still exhibits its total pressure character as shown by the blue loss core. The tip vortex core starts diffusing at *x/c=0.90* but it is still highly visible in the cross stream plane.

3.4 The total pressure field and losses at exit plane : Figure 10 presents the relative total pressure distribution at the exit plane behind the blade row for all pressure side extension designs. The exit plane is defined as the plane that is normal to the main flow direction at 120% chord length as shown in Figure 10. At this axial position, the tip leakage vortex, the wake and the passage vortex fluid show strong turbulent mixing and diffusive character. The local level of the relative total pressure coefficient can be related to the amount of aerodynamic losses originating from various tip treatments presented in this paper. The aerodynamic losses originating from the dissipation of the mean kinetic energy into thermal energy can be estimated by using local relative total pressure in an isothermal viscous flow simulation in the relative frame of reference. The red color shows the relative total pressure at the inlet of the rotor indicating the lowest loss level. Dark blue indicates the highest level of losses at the exit plane. The best approach to quantify the effectiveness of a tip treatment is to calculate the mass averaged relative total pressure coefficient over the area of interest in the exit plane. The specific area chosen for the evaluation of various tip extensions is the area in the last 25 % of the blade height.

$$\Delta C_{P0,last\ 25\%\ blade\ height} = \overline{C}_{P0,exit\ plane} - \overline{C}_{P0,inlet}$$
$$\Delta C_{P0} = \Delta C_{P0,last\ 25\%\ blade\ height} \qquad (9)$$

This area fully contains the leakage flow dominated zone and a significant portion of the blade wake and core fluid between the wakes. Since the leakage vortex and passage vortex has a significant interaction in the passage, the rest of the passage is affected from this interaction. Slight variations in the blade wakes is closely related to the flow structure change in the tip leakage area. Table 2 presents the area averaged total pressure loss as the difference of total pressure loss coefficients between the exit plane and inlet plane in the relative frame of reference.

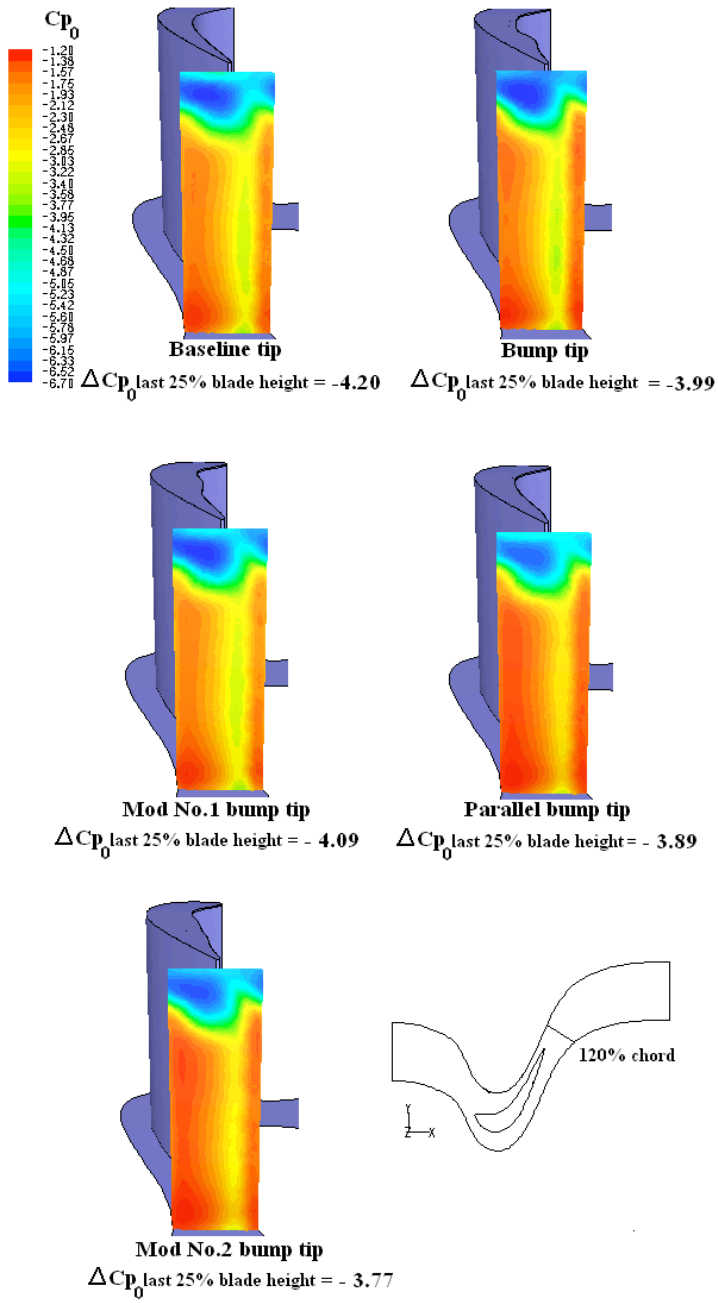

Figure 10 *Total pressure coefficients at the exit plane*

The "*bump tip*" flow modifications provide a good improvement when compared to the baseline case as shown in Figure 10 and Table 2. This computational result is consistent with the experiments performed in the same turbine rig ss level of ΔC_{P0}=-3.99 is obtained from the bump tip. The "*baseline tip*" loss level is at ΔC_{P0}=-4.20 .

The "*parallel extension tip*" based on the idea that a much longer tip extension in chordwise direction is likely to provide more effective tip loss control. The flow computations show a slightly better loss control than the baseline case. However the parallel extension tip does not by Dey and Camci (2004). An aerodynamic lo

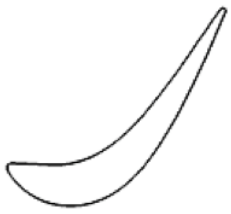 Baseline tip	 Bump tip
$\Delta C_{P0} = -4.20$	$\Delta C_{P0} = -3.99$
 Parallel bump tip	 Mod bump no.1 tip
$\Delta C_{P0} = -4.09$	$\Delta C_{P0} = -3.89$
 Mod bump no.2 tip	
$\Delta C_{P0} = -3.77$	

Table 2 *Comparison of aerodynamic losses (change in non-dimensional relative stagnation pressure)*

perform as well as the bump tip. [ΔC_{P0}=-4.09]

The "*modified bump No.1 tip*" is a design to test the location of the maximum bump location. When the maximum bump location is moved to a mid chord position, a significant loss control is achieved when compared to baseline, bump, parallel bump tip designs. [ΔC_{P0}=-3.89]

The "*modified bump No.2 tip*" is a design combining the benefits of the "*bump tip*" and the "*modified bump No.1 tip*" design as shown in Figure 1.e. This design provides the most significant gain in terms of controlling the tip aerodynamic losses. A ΔC_{P0} of -3.77 results in when compared to that of the baseline case ΔC_{P0}=-4.20.

4 CONCLUSION

The current study presents computational viscous flow simulations of various tip platform extension designs for the control of aerodynamic losses originating from tip leakage flows in an axial flow turbine.

The present computational results are flow simulations that are obtained for turbine experiments performed by Dey and Camci (2004) in AFTRF.

Carefully measured rotor inlet conditions and rotor geometry are used in the linear cascade simulations of AFTRF rotor conditions in the relative frame of reference.

The four new tip platform designs are compared to the AFTRF baseline blade tip that does not have any tip platform extensions. All four cases show measurable improvement in reducing tip leakage related losses.

The quantitative estimations of the over tip leakage flow are achieved by calculating the mass flow rate across the mean camber line region. All of the pressure side extension tips produce reduced mass flow rates across the mean camber line region. The most effective tip geometry to reduce the mass flow rate across the camber line region is the "*modified bump No.2 tip*".

The flow leakage patterns at 3 chordwise visualization planes are presented to show that the pressure side extension tips are able to weaken the tip vortex structure.
The "*bump tip*" flow modifications provide a good level of loss reduction when compared to the baseline case. This computational result is consistent with experiments performed in the same turbine rig by Dey and Camci (2004).

The "*parallel extension tip*" provides more effective tip loss control. The flow computations for this case show a slightly better loss control than the '*baseline case*". However, the "*parallel extension tip*" does not perform as well as the "*bump tip*". [ΔC_{P0}=-4.09]

The "*modified bump No.1 tip*" is obtained when the maximum bump location is moved to a mid chord position. A significant loss control is achieved when compared to baseline, bump and parallel bump tip designs. [ΔC_{P0}=-3.89]

The "*modified bump No.2 tip*" is a design combining the leakage control benefits of the "*bump tip*" and the "*modified bump No.1 tip*" design. This design provides the most significant aerodynamic loss reduction.

The prediction of the aerodynamic losses in the absolute frame of reference including all rotational flow effects and an annular geometry is currently in progress. This future

viscous flow study includes a complete NGV stationary flow simulation and a blade passage computation that is connected to stationary frame through a mixing plane analysis.

Aerothermal and structural aspects of integrating tip platform extensions into hot turbine environment is a topic for future study in our laboratory. The feasibility of the current aerodynamic design needs to be demonstrated for the hot gas environment.

NOMENCLATURE

c	Axial chord = c= 0.0864 m Actual chord=0.1193 m
C_d	Discharge coefficient, ratio of actual to ideal mass flow
C_p, C_{p0}	Static and total pressure coefficients
ΔC_p	Aerodynamic loss coefficient
C_μ	Constant, 0.09
E	Empirical constant, 9.793
t	Tip clearance
h	Rotor blade height
k	Turbulent kinetic energy
K	von Karman's constant
k_p	Turbulence kinetic energy at point p
N	Turbine rotational speed rpm
P_{total}	Total pressure
P	Static pressure
P_{inlet}	Rotor inlet static pressure
RANS	Reynolds averaged Navier-Stokes
r, θ, x	Radial, tangential and axial coordinates respectively
s	Pitch
s/c	Pitch to chord ratio=0.833
t	Tip clearance
u_i	Fluctuating velocity component
U_i	Mean velocity component
U_m	ω.r at blade mid span
u_p	Mean velocity of the fluid at point p
V_2	Relative exit velocity
V_p	Pressure side velocity
V_s	Suction side velocity
y_p	Distance from point p to the wall
x,y,z	Cartesian coordinate system
β	Relative angle
ε	Turbulent dissipation rate
ρ	Density
μ	Viscosity
μ_t	Turbulent (or eddy) viscosity
ξ	Kinetic energy loss coefficient
σ_k	Constant, 1

REFERENCES

Bindon, J.P., 1988, "The Measurement and Formation of Tip Clearance Loss," ASME 88-GT-203.

Bindon, J.P. and Morphis, G., 1990, "The Development of Axial Turbine Leakage Loss for Two Profiled Tip Geometries Using Linear Cascade Data," ASME 90-GT-152.

Booth, T.C., 1985, "Tip Clearance Effects in Axial Turbomachines," VKI Lecture Series 1985-05.

Camci, C., Dey, D. and Kavurmacioglu, L., 2005, "Aerodynamics of Tip Leakage Flows Near Partial Squealer Rims in an Axial Flow Turbine Stage," Transactions of the ASME Journal of Turbomachinery, Vol. 127, No.1, pp. 14-24.

DeCecco, S., Yaras, M.L. and Sjolander, S.A., 1995, "Measurements of the Tip-Leakage Flow in a Turbine Cascade with Large Clearances," ASME 95-GT-77.

Denton, J.D., 1993, "Loss Mechanisms in Turbomachines," ASME 93-GT-435.

Denton, J.D. and Cumpsty, N.A., 1987, "Loss Mechanisms in Turbomachines," Inst. Mech. Eng. paper C260/87.

Dey, D. and Camci, C., 2004, "Tip Desensitization of an Axial Turbine Rotor Using Tip Platform Extensions," VKI Lecture Series 2004-02.

Harvey, N.W. and Ramsden, K., 2000, "A computational Study of a Novel Turbine Rotor Partial Shroud," ASME 2000-GT-668.

Heyes, F.J.G., Hodson, H.P. and Dailey, G.M., 1991, "The Effects of Blade Tip Geometry on the Tip Leakage Flow in Axial Turbine Cascades," ASME 91-GT-135.

Kavurmacioglu, L., Dey, D., and Camci, C., 2004, "Aerodynamic Character of Partial Squealer Tip Arrangements in an Axial Flow Turbine," VKI Lecture Series 2004-02.

Lakshminarayana, B., Camci, C., Halliwell, I., and Zaccaria, M., 1992, "Investigation of Three Dimensional Flow Field in a Turbine Including Rotor/Stator Interaction. Part I: Design Development and Performance of the Research Facility," AIAA paper 92-3326.

Patel, K.V., 1980, "Research on a High Work Axial Gas Generator Turbine," SAE 800618.

Prakash, C., Lee, C.R., Cherry, D.G., Doughty, R. and Wadia, A.R., 2006, "Analysis of Some Improved Blade Tip Concepts," Transactions of the ASME Journal of Turbomachinery, Vol. 128, No. 1, pp. 639-642.

Yamamoto, A., Tominga, J., and Matsunuma, T., 1994, "Detailed Measurements of Three-Dimensional Flows and Losses Inside an Axial Flow Turbine Rotor," ASME 94-GT-348.

Yaras, M.I. and Sjolander, S.A., 1991, "Measurements of the Effects of Winglets on Tip-Leakage Losses in a Linear Turbine Cascade," ISABE 91-7011, pp. 127-135.

Zaccaria, M. and Lakshminarayana, B., 1995, "Investigation of Three-Dimensional Flowfield at the Exit of a Turbine Nozzle," AIAA Journal of Propulsion and Power, Vol.11, No.1, pp. 55-63.